Open Access Journal

Journal of Sustainable Research in Engineering Vol. 2 (2) 2015, 63-69

Journal homepage: www.jkuat-sri.com/ojs/index.php/sri/index

Strain Rate Effects on the Tensile Behavior of Fiber Bundles Isolated from Nerve Root

Atsutaka Tamura[*1], Junji Murakami[1], Yuta Sone[1] and Takao Koide[1]

[1]*Department of Mechanical and Aerospace Engineering, Graduate School of Engineering, Tottori University, Koyama 4-101, Tottori 680-8552, Japan.*

[*]*Corresponding Author - E-mail: a-tamura@mech.tottori-u.ac.jp*

Abstract Fresh porcine spinal cords (N = 5) were obtained at a local abattoir, and intact nerve roots were excised at cervical, thoracic, and lumbar levels using a surgical scalpel and fine forceps with a special caution. In total, 77 fiber bundles with a dimension of 30 mm in length and 0.5 mm in diameter were isolated from the excised nerve roots. By conducting a series of uniaxial stretching tests at three different velocities, 0.1, 1, and 10 mm/s, we revealed that mechanical properties of fiber bundles were relatively insensitive to strain rates under such a sub-impulsive loading condition. On average, elastic moduli, linear portion of stress–strain curve, resulted in 3.8, 3.3, and 4.5 MPa for 0.1, 1, and 10 mm/s, respectively. In addition, strain at failure was almost constant, ~0.15, irrespective of a 100-fold increase in the applied loading rate, while at the same time axial strains were distributed non-homogeneously along fiber direction. We also found that spinal level effect may exist in the spinal nerve roots, suggesting that we should pay more close attention even to an anatomical site where excised samples are obtained.

Keywords nerve root, fiber bundle, uniaxial stretch, whiplash injury, automotive crash.

1. Introduction

Whiplash injury, one of the typical traffic injuries involved with automotive accidents, is a world-wide health concern. Since inflicted trauma of the nervous system is likely to cause a long-term impairment or permanent disability, whiplash injury may result in a deterioration of the patient's quality of life in addition to a high societal cost relevant to the medical treatment. However, a specific mechanism of whiplash or the source of pain associated with it is yet to be clarified. With regard to an anatomical structure, the spinal cord is directly or indirectly protected by the three-layered meninges and "cushion-like" cerebrospinal fluid filling the subarachnoid space, while it is physically supported by the nerve roots inside the spinal canal, i.e., a series of nerve roots locating along both sides of the spinal cord play an essential role in limiting its physiological ranges of motion in the spine. Thus, it would be possible that traumatic loading condition experienced in an automotive crash leads to a mechanical and functional damage of the nerve roots and results in whiplash-associated disorders. In recent years, it is common to utilize a mathematical human body model to predict blunt trauma involved with traffic accidents [1]–[3]. In terms of an injury prediction, it is critically important to incorporate accurate mechanical properties into mathematical models to produce a "reasonable" and biofidelic response. But accurate characterization of nerve root, which provides important data for advanced numerical modeling, has not been adequately addressed. In the present study, we assumed that a mechanical stretch is applied to the nerve roots when an impulsive neck flexion/extension movement occurs during rear-end collision, resulting in an acute or chronic pain by exceeding some "critical" point. Hence, as a first step, this study aimed to measure the mechanical properties of the nerve roots by performing a uniaxial tensile test at elongation rates relevant to sub-impulsive loading condition.

2. Materials and Methods

2.1. Sample preparation

Fresh porcine spinal cords (N = 5) were procured at a local abattoir immediately after sacrifice and were carried back to the laboratory with ice packs. The intact nerve roots, locating along both sides of the spinal cord, were excised using a surgical scalpel and fine forceps at room temperature with a special caution and kept in a physiological saline to avoid dehydration. Further, nerve roots were stored in a refrigerator overnight (12 h) at 4°C in a 50% (v/v) glycerol physiological saline solution. Biological materials stored in this manner have been shown to have stable mechanical properties [4]–[6], and stored samples showed no signs of deterioration at the macroscopic scale in the current work. For dissection of fiber bundle samples, nerve roots were removed from the storage solution and transferred into a dish filled with the physiological saline. Single fiber bundles with a dimension of 30 mm in length and approximately 0.5 mm in diameter were carefully separated from the nerve root using fine forceps and a dissecting needle, and were subsequently kept in the physiological saline solution in the ice-cold box until the experiment.

2.2. Mechanical Testing

The isolated specimen was mounted on a custom-made test apparatus integrated with a pair of parallel-plate load cells (Fig. 1), which is capable of applying 40 mm stretch at a maximum rate of 20 mm/s. One strain gauge (UFLK-1-11, Tokyo Sokki Kenkyujo) was glued onto each side of the thin stainless steel plates (50 mm long × 10 mm wide × 0.1 mm thick) and the half-bridge circuit, i.e., the two active gauge method, was set up. The custom-made parallel-plate cantilever arms were then attached to a pair of linear motors (XMSG430, Suruga Seiki) that controlled the specimen length with a controller driven in a half-step mode (MSCTL102, Suruga Seiki). These arms acted as sensitive force transducers, i.e., channels 1 and 2, and zero strain for performing data analysis was defined later as the point where the sum of the forces in channels 1 and 2 constantly exceeded 0.2 mN. Force data was recorded using a commercial data acquisition system (NR-ST04R, Keyence) at 1 kHz per channel.

An image of the fiber bundle was captured using a digital camera (EX-ZR400, Casio) from both top and side views with a mirror inclined at 45° angles to measure the specimen's length, width, and height; a movie was recorded at 30 fps during each test to produce consecutive still images for post-processing image analysis. To synchronize the timing of the captured image and force data, an LED light was brought into the field of observation view and was manually turned on when we started testing. The driving voltage of the LED was also recorded in the data acquisition system (NR-HA08, Keyence) and used to match the timing of the turning-on of the LED in the video.

Additionally, both ends of the specimen were glued to the cantilever arm tips using cyanoacrylate adhesive and immersed into the warmed physiological saline. Each of the specimens was manipulated very carefully to avoid uncontrolled stretching and severe torsion. The innermost initial distance between the grips was adjusted to 18 mm while maintaining the suspended fiber bundle almost horizontally using micrometers attached to the linear motors such that the stretch was applied purely in the fiber axial direction. Vanilla beans were placed along the longitudinal axis of isolated fiber bundles at approximately 1-mm intervals and used as markers to monitor local strains (Fig. 2). Further, each specimen was divided into 10–12 segments, numbered from one to 10–12 along the axial fiber direction.

As shown in Figure 3, a typical loading path consisted of six cycles of preconditioning, 60-s rest, and a final stretch up to failure. In the preconditioning cycle, uniaxial stretch was applied to a fiber bundle at a rate of 1 mm/s until it reached approximately 10% strain (4-mm displacement). After a complete recovery of residual slack during the rest time, the final stretch was applied at either of the three different velocities, 0.1 mm/s (0.006 s^{-1}), 1.0 mm/s (0.06 s^{-1}), or 10 mm/s (0.6 s^{-1}), so that local strains progressively increased until failure. Samples were discarded if any irregularities were observed along their length during testing or if they were damaged or if they slipped at either of the attachment points during the preconditioning cycle. At the end of an experiment, any fiber bundle that had distinct tears or disruptions at the attachment points was also rejected. Consequently, 36 of 77 specimens were rejected based on these criteria. The temperature of the specimen bath was maintained at 37°C with a hot plate (TP-SP, Tokai Hit). All the experiments were completed within 12 h after specimens were prepared.

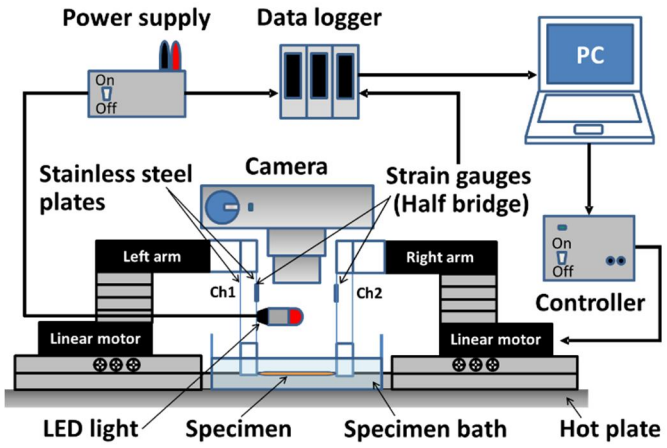

Fig. 1. Schematic view of a custom-made uniaxial tensile tester.

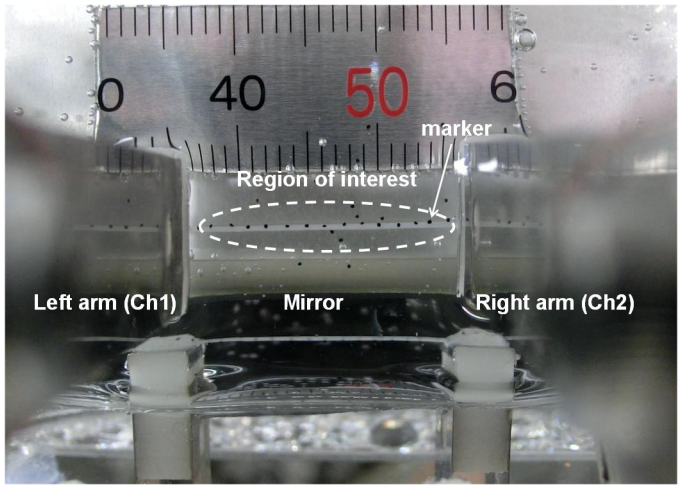

Fig. 2. Magnified region of interest subjected to a dynamic uniaxial stretch.

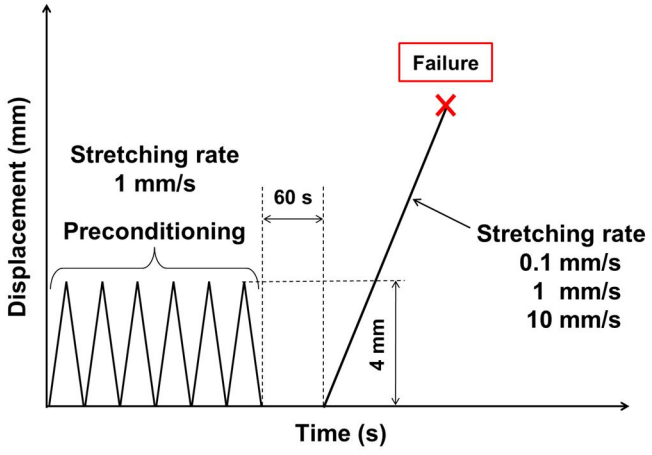

Fig. 3. Test protocol consisting of a set of preconditioning cycles, 60-s rest, and final stretch up to material failure.

2.3. Data Analysis

After the experiment, sample dimensions were measured with an image processing software (ImageJ, NIH). Stress was obtained as the force divided by the initial cross-sectional area, assuming a cylindrical shape of the specimen, and the fiber cross-sectional area was calculated as the mean of three individual measurements at the central region of the fiber bundle. Further, axial strain of each segment along the fiber bundle was obtained as the stretch ratio, the current length divided by the initial length stipulated between two adjacent markers; "strain" for depicting a stress–strain curve was then calculated as the mean value of a series of local axial strains obtained for each fiber bundle.

3. Results

3.1. Axial Strain Distribution

A typical transient changes in axial strain up to failure obtained in a final stretch is shown in Figure 4. Even in a relatively low-rate loading condition at 1 mm/s (0.06 s^{-1}), the applied stretch was distributed non-uniformly along the fiber bundle, resulting in random disparity of axial strains among divided segments or strain concentration in a specific site. Some of the regions appeared to lengthen substantially just before failure, possibly due to the concentration of micro-damage caused by overstretching. However, averaged stretch at failure was almost constant irrespective of a 100-fold increase in the applied loading rate (Fig. 5); the specimens failed at stretch ratios of 1.15 ± 0.03, 1.13 ± 0.02, and 1.17 ± 0.02 (mean ± SD) on average, for strain rates of 0.006, 0.06, and 0.6 s^{-1}, respectively, indicating that the fiber bundles were elongated almost uniformly from a macroscopic point of view and failed at a random site. Moreover, we found that averaged strains among divided segments were almost the same as that obtained from the length change between two markers placed at both ends, i.e., a measurement error fell within a range of 0.5% during the loading phase up to failure. Thus, in the following analysis, fiber strains were calculated based on the length change stipulated by both end markers.

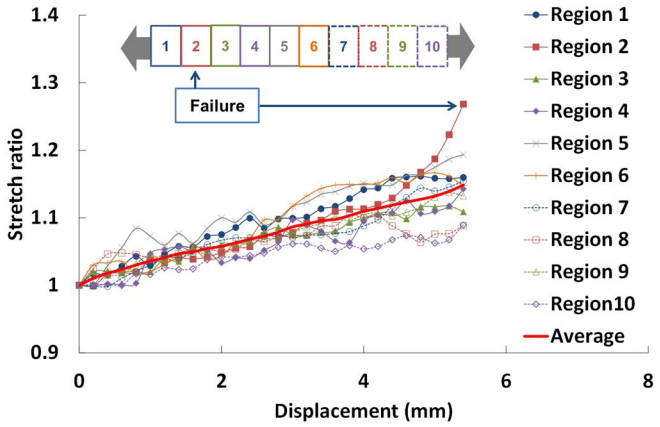

Fig. 4. Typical transient changes in axial stretch ratio among divided segments; each data was obtained from a fiber bundle isolated from lumbar spinal nerve root stretched at 1 mm/s.

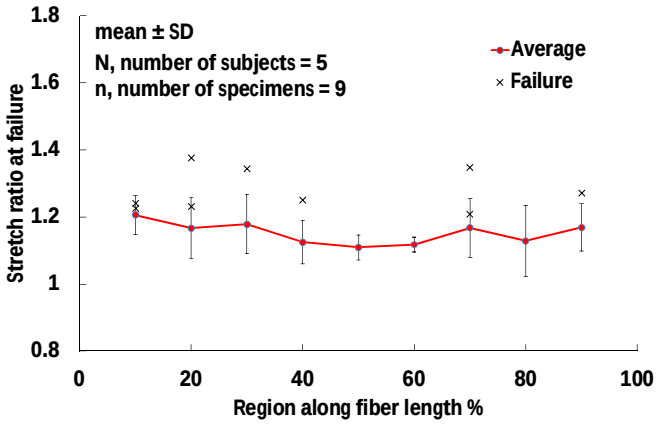

(a) 0.1 mm/s (0.006 s^{-1}).

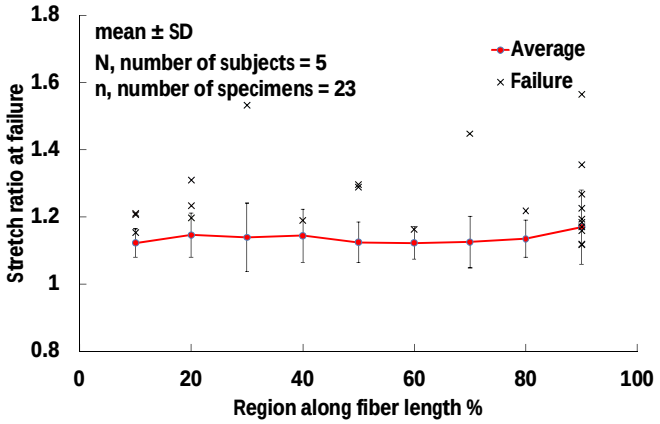

(b) 1 mm/s (0.06 s^{-1}).

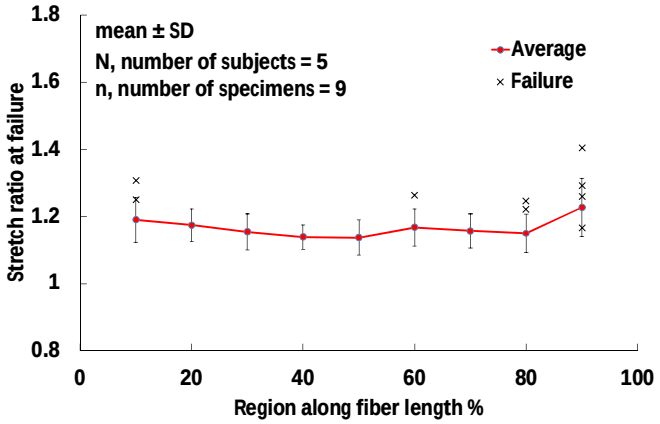

(c) 10 mm/s (0.6 s^{-1}).

Fig. 5. Stretch distribution along fiber length just before failure.

3.2. Tensile Behavior

Figure 6 demonstrates a series of stress–strain curves obtained at three different loading rates. As is common for biological soft tissues, a toe-region was observed early in the loading phase. As shown in Table 1, the tensile strength was significantly higher for specimens stretched at 10 mm/s (0.6 s^{-1}) compared to those stretched at the relatively moderate loading rates, 1 mm/s (0.06 s^{-1}) and 0.1 mm/s (0.006 s^{-1}). In addition, significant difference was observed for failure strain between the groups stretched at 1 and 10 mm/s. Furthermore, apparent elastic moduli for each of the test conditions were calculated as shown in Table 2. To approximate the obtained stress–strain curve as a bilinear function, Young's moduli E_1 and E_2 were defined for the toe region (0–5% strain) and the linear part ($\varepsilon > 5\%$ strain up to failure), respectively. The elastic moduli obtained at the moderate loading rates, 0.1 mm/s (0.006 s^{-1}), 1 mm/s (0.06 s^{-1}), and the high loading rate, 10 mm/s (0.6 s^{-1}), were favorably comparable in low as well as high strain regions. However, the elastic moduli obtained for linear region, E_2, were significantly different between the groups stretched at 1 and 10 mm/s (Table 2).

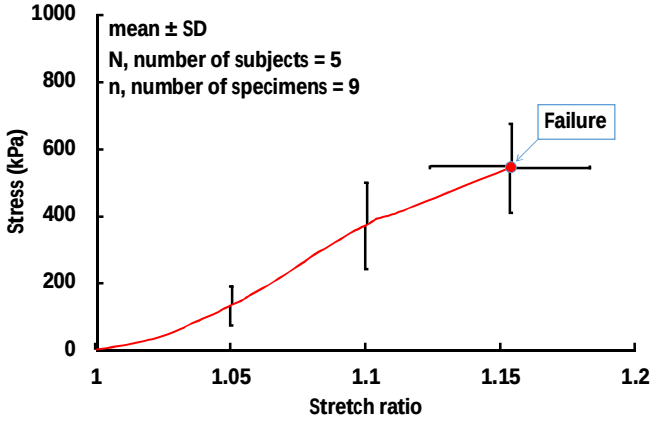

(a) 0.1 mm/s (0.006 s^{-1}).

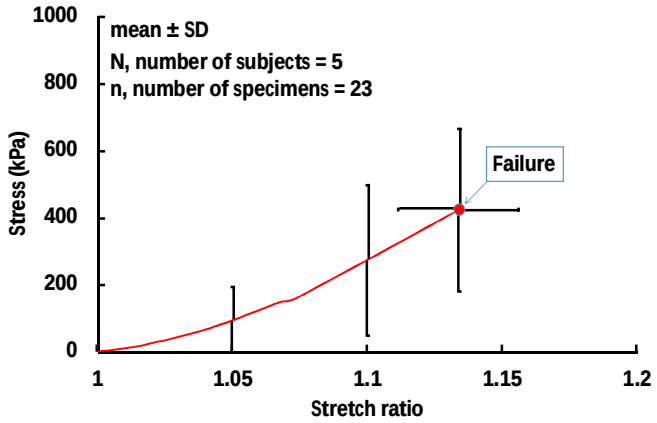

(b) 1 mm/s (0.06 s^{-1}).

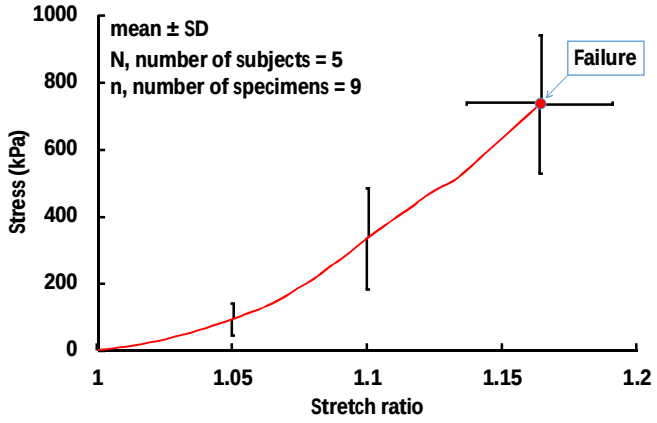

(c) 10 mm/s (0.6 s^{-1}).

Fig. 6. Stress–stretch ratio curves obtained for a series of dynamic uniaxial stretching tests

Table 1: Tensile strength and failure stretch obtained for three different loading rates (mean ± SD).

Stretch rate (mm/s)	*n* (*N* = 5)	Tensile strength (kPa)		Failure stretch	
0.1	9	543 ± 132		1.15 ± 0.03	
1	23	430 ± 242	**	1.13 ± 0.02	**
10	9	713 ± 178		1.17 ± 0.02	
			*		

Asterisks indicate a statistical significance, i.e., *$P < 0.05$ and **$P < 0.01$.

Table 2: Elastic moduli of toe and linear regions obtained for three different loading rates (mean ± SD).

Stretch rate (mm/s)	*n* (*N* = 5)	E_1 (MPa)	E_2 (MPa)	
0.1	9	2.95 ± 1.15	3.80 ± 1.07	
1	23	2.34 ± 1.86	3.26 ± 2.03	*
10	9	2.06 ± 0.94	4.49 ± 1.07	

Asterisks indicate a statistical significance, i.e., *$P < 0.05$ and **$P < 0.01$.

3.3. Spinal Level Effect

Out of the 41 fiber bundles isolated from spinal nerve roots, 23 specimens subjected to stretch at a rate of 1 mm/s ($N = 4$) were selected and divided into three groups based on the anatomical sites or spinal levels where specimens were excised; mechanical properties of the nerve roots were then evaluated at cervical, thoracic, and lumbar levels (independent *t*-tests). As summarized in Table 3, stretch at failure was obviously independent of spinal levels. No significant differences were found between cervical and thoracic spinal levels in tensile strength and elastic moduli, either (Tables 3 and 4). On the other hand, tensile strength was significantly higher in cervicothoracic spinal levels as compared to lumbar spinal level ($P < 0.01$). The elastic moduli were also found to be higher in cervicothoracic spinal levels as compared to lumbar spinal level.

Table 3: Tensile strength and failure stretch obtained for each of spinal levels at the stretching rate of 1 mm/s (mean ± SD).

Spinal level	*n* (*N* = 4)	Tensile strength (kPa)		Failure stretch	
Cervical	5	609 ± 145		1.15 ± 0.02	
Thoracic	7	610 ± 169	**	1.13 ± 0.02	**
Lumbar	11	236 ± 168		1.13 ± 0.02	
			**		

Asterisks indicate a statistical significance, i.e., *$P < 0.05$ and **$P < 0.01$.

Table 4: Elastic moduli of toe and linear regions obtained for each of spinal levels at the stretching rate of 1 mm/s (mean ± SD).

Spinal level	*n* (*N* = 4)	E_1 (MPa)		E_2 (MPa)	
Cervical	5	2.61 ± 1.19		4.25 ± 1.07	
Thoracic	7	4.03 ± 2.27	**	4.80 ± 2.02	**
Lumbar	11	1.15 ± 0.61		1.83 ± 1.34	
			*		**

Asterisks indicate a statistical significance, i.e., *$P < 0.05$ and **$P < 0.01$.

4. Discussion

The accurate mechanical characterization of biological soft tissues is critically important to well predict traumatic injuries using a computational model. However, available data obtained at high loading rates is considerably limited due to the technical difficulties involved in handling the soft tissue materials. In the present study, we performed a series of uniaxial stretching tests using fiber bundles isolated from porcine nerve roots. We investigated mechanical properties of fiber

bundles by applying the sub-impulsive loading rates ranging from 0.1 to 10 mm/s; typical stress–strain curves of biological soft tissues with a toe region followed by a linear region were obtained (Fig. 6), which can be simply approximated by a bilinear function. As we expected, a statistical significance ($P < 0.01$) was found in tensile strength between the high (10 mm/s) and moderate loading rates (0.1 and 1 mm/s). But contrary to our expectation, neither the elastic moduli, nor the stretch at failure were strongly sensitive to tensile velocities given here (Tables 1 and 2), although there was a 100-fold increase in the applied loading rate, i.e., nerve roots are inherently insensitive to stretching velocity under sub-impulsive loading rates. It should be noted, however, that the tensile strength was significantly different between cervicothoracic and lumbar spinal levels at the rate of 1 mm/s (Table 3), suggesting that there is some spinal level effect in the mechanical strength of nerve roots. This might be reasonable when an anatomical structure of the spinal cord is considered, i.e., since the spinal cord is directly connected to the brain, the heaviest organ in the central nervous system, it is more likely that nerve roots of the cervicothoracic levels are constantly exposed to mechanical stretch due to a daily motion or activity rather than those of the lumbar spinal level.

Singh et al. [7] evaluated biomechanical properties of rat dorsal nerve roots at the lumbar and sacral levels using two different stretching rates, 0.000833 s^{-1} (0.01 mm/s) and 1.25 s^{-1} (15 mm/s). With regard to maximum stress and elastic modulus of linear portion in stress–strain curve, they revealed that higher values occurred at the dynamic loading rate as compared to those at quasi-static loading rate, indicating that strain rate dependency exists in the spinal nerve roots. In more specific, dorsal nerve roots subjected to a mechanical stretch resulted in a maximum stress of 258 ± 111 kPa and elastic modulus of 1.3 ± 0.8 MPa for 0.01 mm/s and 625 ± 307 kPa and 2.9 ± 1.5 MPa for 15 mm/s, respectively. Significant differences in mechanical behavior were also observed among the four root levels (L4, 5, 6 and S1) where each of the specimen was isolated. However, no statistical difference was found in the strain values at failure even though there was a 1500-fold increase in the applied loading rate. Similar to their work, in the present study, an averaged regional stretch distribution along axial fiber direction that we obtained was almost consistent just prior to failure (Fig. 5), although axial strains were distributed non-uniformly along the fiber length even in the moderate loading rate, 1 mm/s (Fig. 4); these results may indicate that fiber bundle fails at the point when an applied stretch reached some “critical” strain.

This study is limited by a couple of reasons. In the current work, testing samples were stored in 50% (v/v) glycerol saline solution for overnight before fiber bundles were isolated from the excised nerve roots. According to the previous studies [4]–[6], glycerol effect on mechanical properties of biological specimens is relatively limited in case the immersion time is well controlled. For instance, van Noort et al. [4] reported that no statistically significant difference was shown in mechanical properties of human dura mater irrespective of time of storage in 98% (v/v) glycerol for 1–12 days. McGarvey et al. [5] also reached a similar conclusion, i.e., storage in 98% (v/v) glycerol for more than two weeks shifted the stress–strain curve to lower strain, however, the mechanical effect of glycerol preservation on human dura mater was not significant for elastic modulus calculated from the linear portion of the stress–strain curve. In addition, Hashimoto et al. [6] characterized compressive properties of porcine cornea and showed that elastic moduli of the cornea were not significantly different between before and after 100% (w/w) glycerol immersion treatment for 1 h. Since glycerol acts as a weak dehydrating agent, long-term glycerol storage is likely to stiffen mechanical responses of biological materials. However, the testing samples we used were immersed in 50% (v/v) glycerol solution for only 12 h, and the mechanical effect of glycerol storage was resultantly minimized as much as possible. In fact, we did not find any specific damage in the specimens by visual inspection; there might be some microscopic damage existed in the tested samples, though.

Another limitation is a protocol for preconditioning. With regard to a set of preconditioning cycles, Cheng et al. [8] suggested that mechanical responses of biological materials were significantly affected by its procedure, e.g., magnitude of applied strain or strain rate or the number of cycles, etc. We adopted six cycles of a 4-mm displacement, which corresponds to ~10% strain of initial reference length or ~70% of failure strain, for preconditioning each of the specimen before conducting an actual test to failure. The preconditioning cycle was given at 1 mm/s irrespective of the loading rate for the subsequent actual tests. Since it is uncertain whether or not the preconditioning procedure that we had implemented was an optimal option, further study will be required in the future.

5. Conclusions

A series of uniaxial tensile tests were conducted with the use of fiber bundles isolated from nerve roots at quasi-static (0.1 mm/s), medium (1 mm/s), and high (10 mm/s) loading rates. We found that strain rate effect was relatively insignificant for mechanical parameters related to tensile behavior, i.e., tensile strength, elastic modulus, and failure strain were almost constant irrespective of a 100-fold increase in the applied stretching rate. Our results also suggested that spinal level effects were of significance in tensile strength and elastic modulus between the specimens obtained at cervicothoracic and lumbar spinal levels. The mechanical data obtained here will be useful to improve a human head-neck complex model and assess the mechanical response as well as the potential for injury by performing a rear-end impact crash simulation.

Acknowledgement

This study was supported in part by a special research grant from the president at Tottori University and from KAKENHI (15K01290) Grant-in-Aid for Scientific Research (C).

References

[1] J. Hasegawa and A. Shiomi, “A study of whiplash injury occurrence mechanisms using human finite element model,” In: Proceedings of 18th International Technical Conference on the Enhanced Safety of Vehicles, Paper #195, 2003, Nagoya (Japan).

[2] D.S. Cronin, “Finite element modeling of potential cervical spine pain sources in neutral position low speed rear impact,” J. Mech. Behav. Biomed. Mater., vol. 33, pp. 55–66, 2014.

[3] A. Tamura, T. Koide, and K.H. Yang, “Effects of ground impact on traumatic brain injury in a fender vault pedestrian crash,” Int. J. Vehicle Safety, vol. 8, pp. 85–100, 2015.

[4] R. van Noort, M. M. Black, T. R. P. Martin, and S. Meaney, “A study of the uniaxial mechanical properties of human dura mater preserved in glycerol,” Biomaterials, vol. 2, pp. 41–45, 1981.

[5] K. A. McGarvey, J. M. Lee, and D. R. Boughner, “Mechanical suitability of glycerol-preserved human dura mater for construction of prosthetic cardiac valves,” Biomaterials, vol. 5, pp. 109–117, 1989.

[6] Y. Hashimoto, S. Funamoto, S. Sasaki, T. Honda, S. Hattori, K. Nam, T. Kimura, M. Mochizuki, T. Fujisato, H. Kobayashi, and A. Kishida, “Preparation and characterization of decellularized cornea using high-hydrostatic pressurization for corneal tissue engineering,” Biomaterials, vol. 31, pp. 3941–3948, 2010.

[7] A. Singh, Y. Lu, C. Chen, and J. M. Cavanaugh, “Mechanical properties of spinal nerve roots subjected to tension at different strain rates,” J. Biomech., vol. 39, pp. 1669–1676, 2006.

[8] S. Cheng, E.C. Clarke, and L.E. Bilston, “The effects of preconditioning strain on measured tissue properties,” J. Biomech., vol. 42, pp. 1360–1362, 2009.